applied sciences

MDPI

Article

New On-Line MFL Testing Method and Apparatus for Winding Mine Hoist Wire Rope

Xiaoyuan Jiang [1], Yanhua Sun [1], Bo Feng [1,*], Mengqi Liu [1], Xiaotian Jiang [1], Ran Li [2,3], Lingsong He [1] and Yihua Kang [1]

[1] School of Mechanical Science & Engineering, Huazhong University of Science and Technology, Wuhan 430074, China; jiangxy@hust.edu.cn (X.J.); yhsun@hust.edu.cn (Y.S.); d202080231@hust.edu.cn (M.L.); noame@126.com (X.J.); helingsong@hust.edu.cn (L.H.); yihuakang@hust.edu.cn (Y.K.)
[2] School of Transportation and Logistics Engineering, Wuhan University of Technology, Wuhan 430063, China; rangly@126.com
[3] Three Gorges Navigation Authority, Yichang 443002, China
* Correspondence: bofeng@hust.edu.cn

Abstract: Based on the introduction and analysis of difficulties encountered during technical inspection of the wire rope of a winding mine hoist (WMH) working at high speed, an open-loop permanent magnet magnetizer was used to simulate and analyze the effect of the structural dimensions of this magnetizer on the magnetic leakage field of a defect, and the results of the simulation analysis were initially verified by experiments. Additionally, in order to keep the axial position of the probe in line with the axial position of the wire rope, a rocker arm was proposed to act in coordination with a motor to drive the clutching open and closed probe, thereby creating an on-line nondestructive testing device to float and track the movement of the wire rope in different directions. Finally, the device was applied to testing of WMH wire rope on site to validate the effectiveness and feasibility of the method.

Keywords: magnetic flux leakage (MFL); permanent magnet magnetizer (PMM); on-line; high speed; wire rope; winding mine hoist (WMH)

check for updates

Citation: Jiang, X.; Sun, Y.; Feng, B.; Liu, M.; Jiang, X.; Li, R.; He, L.; Kang, Y. New On-Line MFL Testing Method and Apparatus for Winding Mine Hoist Wire Rope. *Appl. Sci.* **2022**, *12*, 6970. https://doi.org/10.3390/app12146970

Academic Editor: Cem Selcuk

Received: 26 February 2022
Accepted: 4 July 2022
Published: 9 July 2022

1. Introduction

Mine hoisting (WMH) wire rope is an essential component for connecting the hoisting conveyance and hoister, as well as a significant tool in the transmission of power. It has been widely used in various industrial fields, including cranes, elevators and metallurgy [1–3]. However, wire rope defects may occur as a result of wear, corrosion, fatigue, broken wire, and other damage, resulting in a decrease in strength or, at times, safety issues and even fatalities [4–6]. The traditional wire rope safety strategy relies mostly on experience and the routine replacement of wire ropes, resulting in greater economic costs and the risk of unexpected abnormal damage during reinstallation, leading to more sudden and serious accidents.

The NDT methods for wire rope include magnetic flux leakage (MFL) testing methods [7,8], ultrasonic testing (UT) methods [9], X-ray inspection [10], acoustic emission (AE) inspection methods [11,12], and eddy current testing (ECT) methods [13]. Among them, the MFL testing method is considered to be the most effective method for detecting wire rope defects [14,15]. For the purpose of enhancing the sensitivity and effectiveness of signal acquisition of leakage magnetic fields at defects, it is necessary for the structural design of the MFL detection device and the magnetic sensitivity sensor to be optimized in order to increase the ability of the MFL device to stimulate leakage magnetic fields at defects and also to increase the ability of the magnetic sensitivity sensor to acquire signals. For example, B Wu [16] used an orthogonal test method (OTM) to optimize the design of an MFL sensor consisting of Helmholtz-like excitation coils, a magnetic shield and a TMR device. Xingliang

Jiang [17] used an improved small-habitat adaptive genetic algorithm to reduce the weight of the detector and improve the robot's carrying capacity. XiaolanYan [18] proposed an iron core as a coil winding skeleton for the nondestructive testing of wire ropes, which altered the MFL path of defects and improved the signal-to-noise ratio of the coil's output. Yiqing Zhang [19] developed a wire rope wire breakage detection sensor based on the magnetic concentration principle and optimized the structural parameters of a toroidal multi-loop permanent magnet exciter (CMPME) to identify external wire breaks in 24 mm diameter wire ropes. Donglai Zhang [20,21] designed a simple and portable magnetic detection device based on a magnetic probe structure to qualitatively and positionally detect wire rope defect. Hongyao Wang [22] proposed a novel magnetic aggregation bridge detection method using magneto resistive (MR) sensor arrays that can detect multiple types of wire ropes damage with a maximum signal-to-noise ratio of 60 dB. W. Sharatchandra Singh [23] developed a flexible GMR array sensor for detecting defects of LF and LMA types on 64 mm diameter wire ropes. The transducer consisting of a fluxgate sensor proposed in [24] demonstrated the feasibility of detecting low frequency and LMA defects in weak magnetic fields with greater sensitivity and better signal-to-noise ratio, compared to Hall elements or induction coils. The fast speed of the wire ropes in operation on the site causes jitter and swings that can cause wear between the wire rope detection sensor and the wire rope; therefore, it was necessary to design a detection sensor with simple structure that is able to adapt to the actual operating conditions of the wire rope.

In order to accommodate jitter and random oscillations among ropes running at high speed, an open-loop permanent magnetization method [25] was used in this study to design an on-line floating tracking testing device incorporating a rocker arm coordinated with an open-close probe. The effect of the magnetizer size and MFL signals of defects was also studied in depth, and the applicability and effectiveness of this online testing device were confirmed through experimental and field testing.

2. In-Service WMH Wire Rope and Its NDT Challenge

The WHM is a traditional hoisting equipment, with one end of the wire rope wound around a winch, and the other end around a guide wheel to adjust the direction of the connection to the transport cage. In the case of wire rope work, as shown in Figure 1, the wire rope is released or retrieved by rotating the winch forward and backward to produce relative movement along the wire rope axis. As the wire rope rotates around the winch, the rope body shakes from side to side and deviates from the central axis, producing the deviation angle θ. Moreover, with changes in tension and speed, the rope sways frequently from the groove of the drum, creating a specific amplitude of δ. Accordingly, along the wire rope axis direction, to establish a spatial coordinate system, the wire rope motion state can be divided into linear motion along the X axis, horizontal wobble along the Y axis, and vertical vibration along the Z axis.

In addition, the surface of the wire rope is coated with oil for protection, and the traditional leakage detection methods (leakage detection devices with magnetic yokes) are not suitable for online high-speed detection due to the small spacing between the wire rope and the wire rope. Otherwise, it will cause scraping oil and wire rope wear, and cannot withstand the friction and impact caused by the relative high-speed movement of the wire rope and the probe, thereby reducing their service life. Therefore, it is necessary to use non-contact measurement methods, and the lifting distance (the distance between the wire rope surface and the probe) should be maintained in order to ensure normal operating conditions in a non-contact setting. Essentially, there are several issues that must be addressed for the on-line detection of wire ropes, as follows:

(1) Probes must be able to open and hold wire ropes for closed-loop structures; therefore, 360-degree closed-loop structures and devices (including excitation and receiving devices) are not available.

(2) Ropes can run at about 15 m/s, and the rope has twining movements at the same time, so any detection method must satisfy the requirements of high-speed operation in addition to tracking movement and ensuring safety.

(3) The dusty environment, dirty oil, complicated vibration movements, and anti-explosion requirements prevent the use of heavy equipment. As a result of maintenance or replacement, a rope's posture may change. Thus, the testing equipment should be capable of automatically adapting to a variety of rope positions.

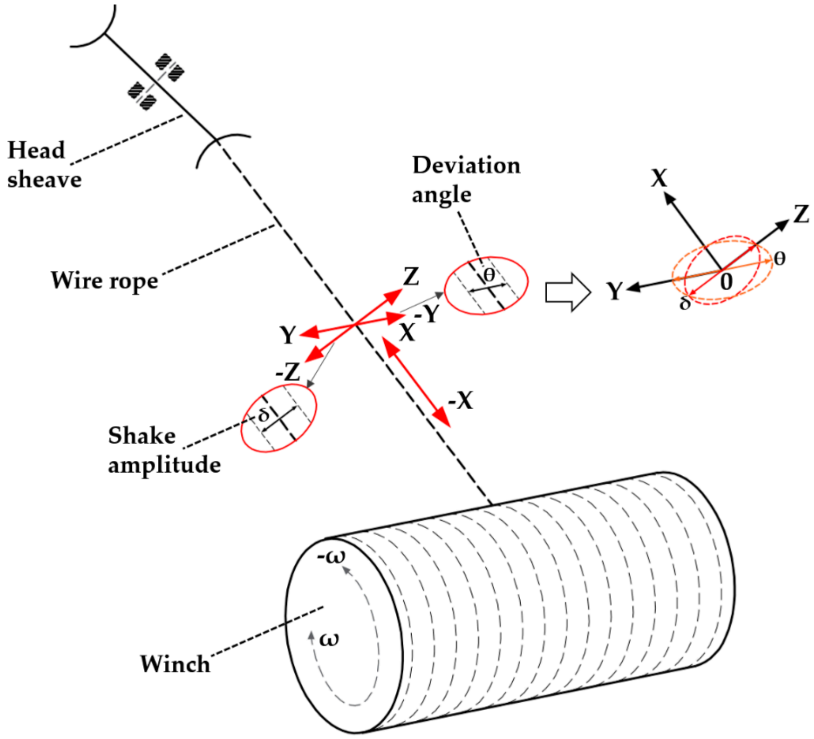

Figure 1. Schematic diagram of the working principle of the WMH system.

3. Analysis of the Novel Probe

3.1. Open-Loop Permanent Magnetizer

In the nondestructive testing of steel wire rope, permanent magnetic leakage detection devices have been widely adopted [14,15]. The three main types of permanent magnetization sensors for steel wire rope are depicted in Figure 2: (a) a sensor of the magnetic bridge type consisting of multiple independent sets of magnetizers [17,26]; (b) a sensor with radial magnetization consisting of two semi-annular sets of upper and lower magnetizers [19,27]; and (c) an open-loop sensor with axial magnetization consisting of upper and lower half-loop magnetizers [25,28].

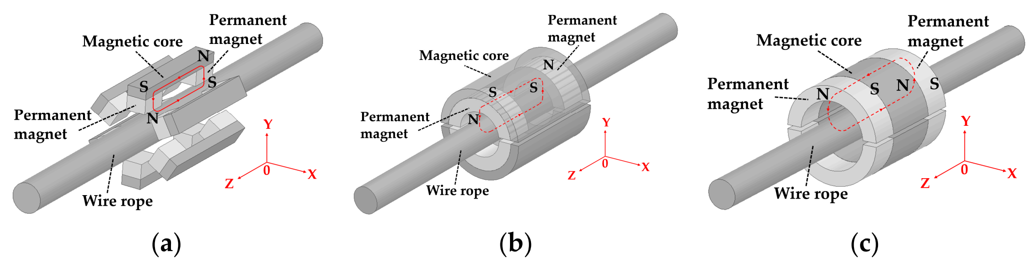

Figure 2. Three types of wire rope permanent magnetization sensors: (**a**) multi-loop magnetic bridge circuit type detection sensor; (**b**) radially magnetized detection sensor; and (**c**) open-loop sensor with axial magnetization.

Magnetic pole surfaces of the detection sensors interact with the corresponding wire rope surfaces, resulting in frictional wear to both the measuring probe and high-speed running wire ropes, making it difficult to distinguish between the probe and the wire rope. In order to analyze the magnetic force applied to the wire rope shown in Figure 2, finite element models were constructed of three detection sensors with the same axial length, diameter, and spacing between magnets. The dimensions and properties of the three sensors are summarized in Table 1.

Table 1. Parameters of the finite element model for the detection sensor.

Parts		Sizes	Material Properties
Wire Rope		Diameter is 30 mm, length is 500 mm.	X52 steel
(a) Six sets of identical magnetic bridge circuit type sensors	Magnets	Length in Z-direction is 30 mm, width in X-direction is 20 mm, height in Y-direction is 15 mm.	NdFeB52
	Magnetic Cores	Length in Z-direction is 120 mm, width in Z-direction is 20 mm, height in Y-direction is 10 mm.	Q235
	Distance between the magnet and the surface of the wire rope	10 mm	
(b) Radially magnetized sensor	Magnets	Inner diameter is 50 mm, outer diameter is 80 mm, thickness is 30 mm.	NdFeB52
	Magnetic Cores	Inner diameter is 80 mm, outer diameter is 100 mm, length is 120 mm.	Q235
	Mating gap between upper and lower magnetizers	4 mm	
(c) Open-loop sensor with axial magnetization	Magnets	Inner diameter is 70 mm, outer diameter is 100 mm, thickness is 30 mm.	NdFeB52
	Magnetic Cores	Inner diameter is 70 mm, outer diameter is 100 mm, thickness is 60 mm.	Q235
	Mating gap between upper and lower magnetizers	4 mm	

Figure 3 illustrates three types of sensors on the wire rope force situation. The magnetic force applied to the wire rope by multiple magnetic bridge sensors is densely distributed and has a large value, while the magnetic force applied by the open-loop sensor with axial magnetization is sparsely distributed and has a very small value. In Table 2, the magnetic force components and the total force generated by the different sensors are shown. The total magnetic force generated by the three magnetizers, (a), (b), and (c), is 29.406 N, 73.263 N and 15.439 N; in other words, the open-loop sensor with axial magnetization applies the smallest magnetic force to the wire rope, which permits high-speed operation of the wire rope by reducing friction between it and the sensor. At the same time, the sensor with a larger inner diameter is located far from the surface of the wire rope, thus enhancing its service life.

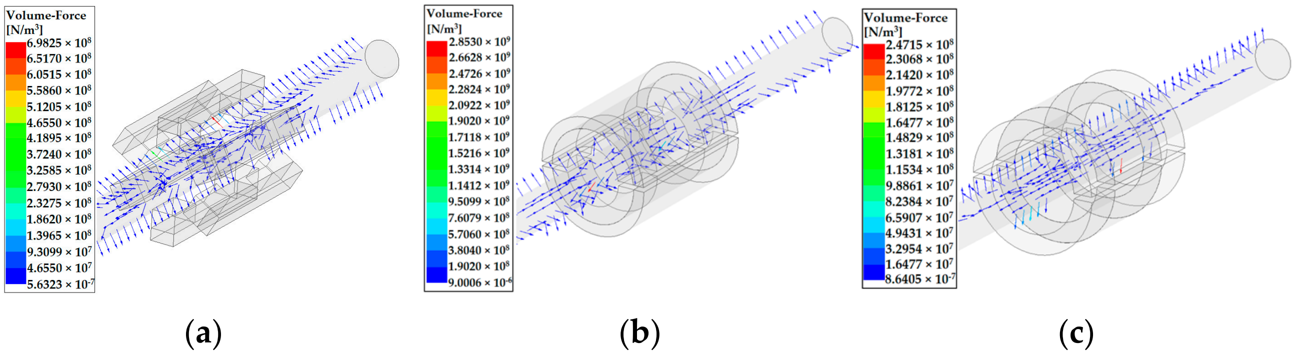

Figure 3. Magnetic force distribution of wire rope under different sensors: (**a**) multi-loop magnetic bridge circuit type detection sensor; (**b**) radially magnetized detection sensor; and (**c**) open-loop sensor with axial magnetization.

Table 2. The components and total of the magnetic force generated by the different sensors.

Magnetizers	The Force Fx in the X-Direction (N)	The Force Fy in the Y-Direction (N)	The Force Fz in the Z-Direction (N)	Total Force Fsum (N)
(a) Six sets of identical magnetic bridge circuit type sensors	19.552	−7.060	−20.798	29.406
(b) Radially magnetized sensor	18.270	−45.756	−54.222	73.263
(c) Open-loop sensor with axial magnetization	12.363	6.658	−6.418	15.439

The structural configuration and detection principle of the open-loop magnetizer are shown specifically in Figures 4 and 5. An open-loop magnetizer is a split structure composed of two identical axially magnetized rings, probe A and probe B, one of which consists of two magnets and a magnetic core to act as a magnetization circuit. The two magnetized rings are placed in the probe housing and combined to form a single unit. The magnetically sensitive elements can be enclosed in ring probe shoes of varying diameters to detect wire ropes of varying diameters. A core is added between the two magnets for strength and mounting of the probe, but the two parts, the magnets and core, can still create a magnetic field for defect detection. The invention provides a device with integrated monetization and signal output, which has the advantages of small size, light weight and compatibility. It can adapt to some specimens with significant shake amplitudes and fast speeds.

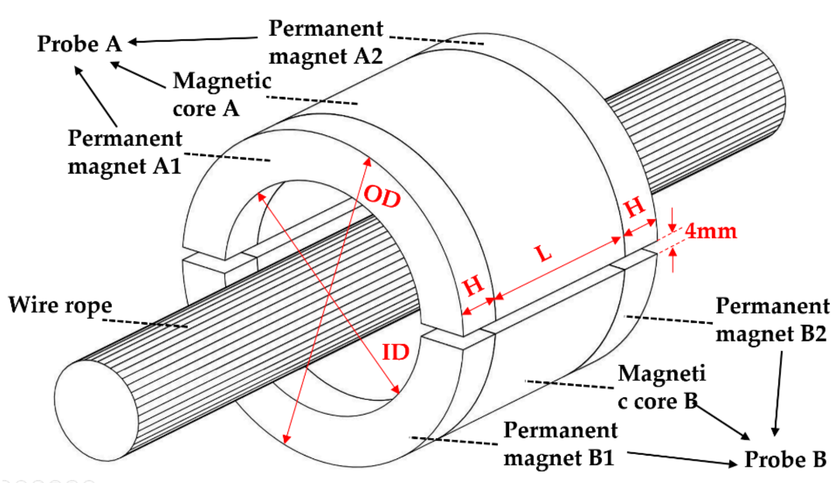

Figure 4. Schematic diagram of the split structures of the probe.

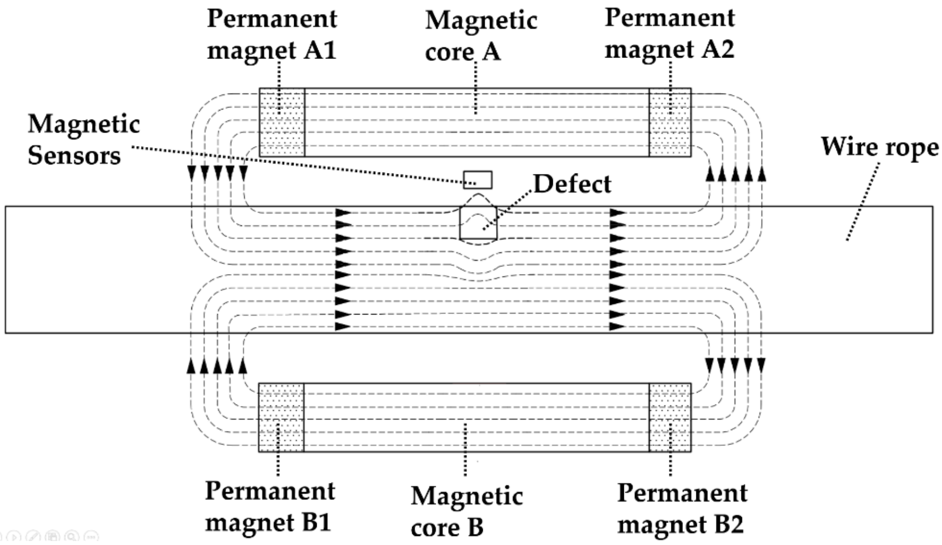

Figure 5. Detection principle of open-loop permanent magnetizers.

According to Kirchhoff's law in the magnetic circuit, the magnetic potential F of a ring-shaped permanent magnet can be expressed as the product of the reluctance and magnetic flux, and when the magnetic flux line passes through the air, the following equation can be obtained:

$$F = \Phi_1 R_{air}, \tag{1}$$

where Φ_1 is magnetic flux outside of the permanent magnet, and R_{air} is the reluctance within the air. When the magnetic flux line passes through the magnetic core and the specimen of the wire rope, we can obtain

$$F = \Phi_2 (R_{left} + R_{specimen} + R_{right}), \tag{2}$$

where Φ_2 is magnetic flux within the permanent magnet and the specimen, and R_{left} and R_{right} are the reluctance within the permanent magnet's left and right-side regions, respectively. By dividing Equation (1) by Equation (2), we can obtain the following relationships:

$$\frac{\Phi_1}{\Phi_2} = \frac{R_{left}+R_{specimen}+R_{right}}{R_{air}}, \tag{3}$$

$$\frac{\Phi_1}{\Phi_1+\Phi_2} = \frac{R_{left}+R_{specimen}+R_{right}}{R_{left}+R_{specimen}+R_{right}+R_{air}}, \tag{4}$$

The total magnetic flux produced by the ring-shaped permanent magnet of Φ_{total} can be described as,

$$\Phi_{total} = \Phi_1 + \Phi_2, \tag{5}$$

Thus, the magnetic dissipation rate λ of the permanent magnet in the new probe could be calculated as,

$$\lambda = \frac{\Phi_1}{\Phi_{total}} = \frac{R_{left}+R_{specimen}+R_{right}}{R_{left}+R_{specimen}+R_{right}+R_{air}}, \tag{6}$$

As Equation (6) shows the ratio of the flux leakage in the air by the excitation source to the total flux provided by the excitation source, in order to reduce the flux leakage in the air, it is necessary to reduce the magnetic dissipation rate λ, i.e., to increase the flux inside the specimen and increase the magnetic saturation rate. The reluctance of R_{air} should be increased, or the parameters of R_{left}, R_{right}, and $R_{specimen}$ should be decreased. As a result, the magnetic energy of the permanent magnet can be fully used.

For the design of the open-loop permanent magnet detection sensor, the finite element method (FEM) simulation is used to analyze the effect of the magnetizer size on the magnetic excitation performance of the defect, as shown in Figure 6. A finite element model is established for a steel bar with a diameter of 30 mm and a length of 1000 mm; the dimensions of the length × width × depth of the defect on its surface are 1 mm × 1 mm × 1 mm; and X52 steel is used as the material property. The MFL detector employs an open-magnetization method with a ring magnet and an intermediate magnetic core to form a magnetization loop, and a gap between the upper and lower magnetizers of the probe is 4 mm to allow for machining and assembly. The material of the magnet is NdFeB N52, which has a coercivity of 955,000 A/m, relative permeability of 1.21, and remanent magnetization of 1.45 T. The material property of the magnetic core is Q235 steel. The ring magnet and magnetic core have the same inner and outer diameters. Considering the magnetizing effect of the permanent ring magnet, the key dimensions of the magnetizer are the inner diameter (ID), the outer diameter (OD), the axial height of the magnet (H), and the axial length of the middle armature (L). The lifting distance is the distance between the magnetic sensing element and the surface of the wire rope. In general, the amplitude of the detection signal decreases rapidly with the increasing lifting distance, so the lifting distance is usually chosen to range from 2 to 10 mm [19,29,30]; however, the lifting height should be as high as possible in order to prevent friction between the device and the wire rope, thus extending the probe's service life. A height of 5 mm was used in this study. In the simulation, the values of ID, OD, H, and L were varied by a single control variable, and the magnetic induction intensity (axial and radial components) was extracted along an axial direction at a height of 5 mm from the defect center of the steel bar surface in order to establish the influence law of size on the defect leakage magnetic field so that an open-loop wire rope leakage magnet detector could be designed to improve the defect detection performance and reduce the design size and weight.

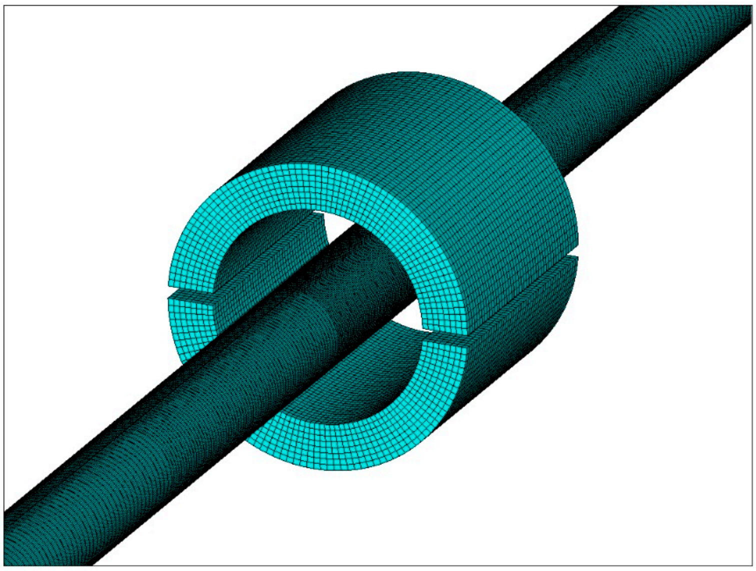

Figure 6. Finite element model of an open-loop permanent magnet magnetizer.

3.2. Simulation Analysis

3.2.1. Variable Is the Axial Length (L) of the Yoke

Select ID = 70 mm, OD = 100 mm, H = 15 mm, the length of the armature (L) varies between 10 and 80 mm. The change curve of defect characteristics is shown in Figure 7: the peak value of defect MFL signal increases first, then decreases as L increases, reaching its maximum value at L = 30 mm.

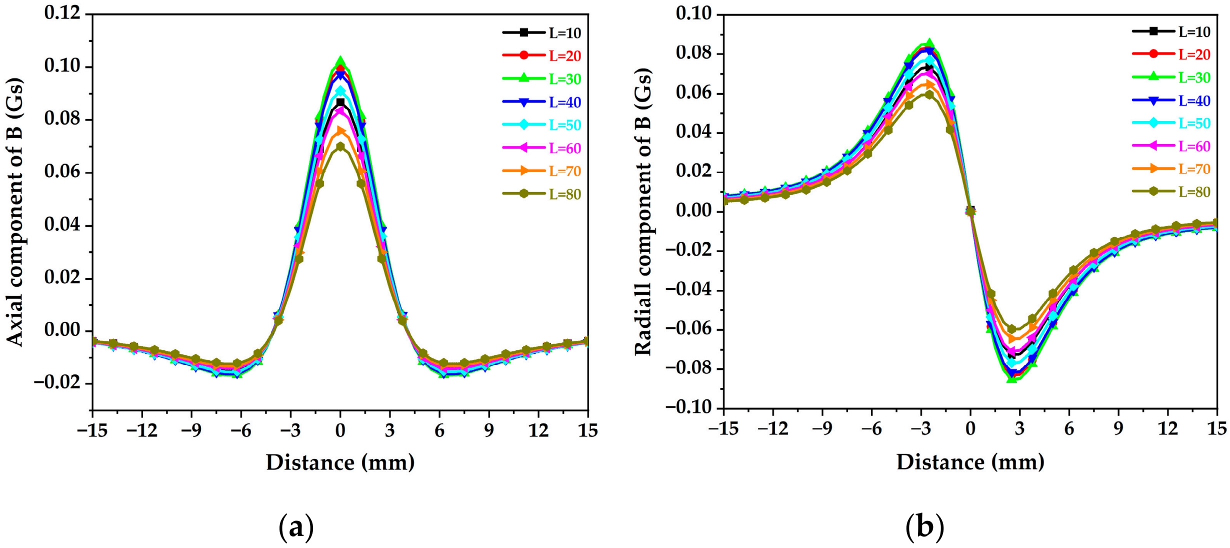

Figure 7. Changes in magnetic flux density with the changed axial length (L) of the yoke: (**a**) axial component of magnetic flux density; and (**b**) radial component of the magnetic flux density.

3.2.2. The Variable Is the Axial Height (H) of the Magnet

Based on the simulation results of Figure 7, the variation curves of the defect characteristics are selected when L = 30 mm, ID = 70 mm, OD = 100 mm, and the axial height (H) of the magnet is varied between 5 and 40 mm, as shown in Figure 8. With the increase in the L value, the peak value of the defect MFL signal increases gradually, and the peak value is maximal when H = 40 mm.

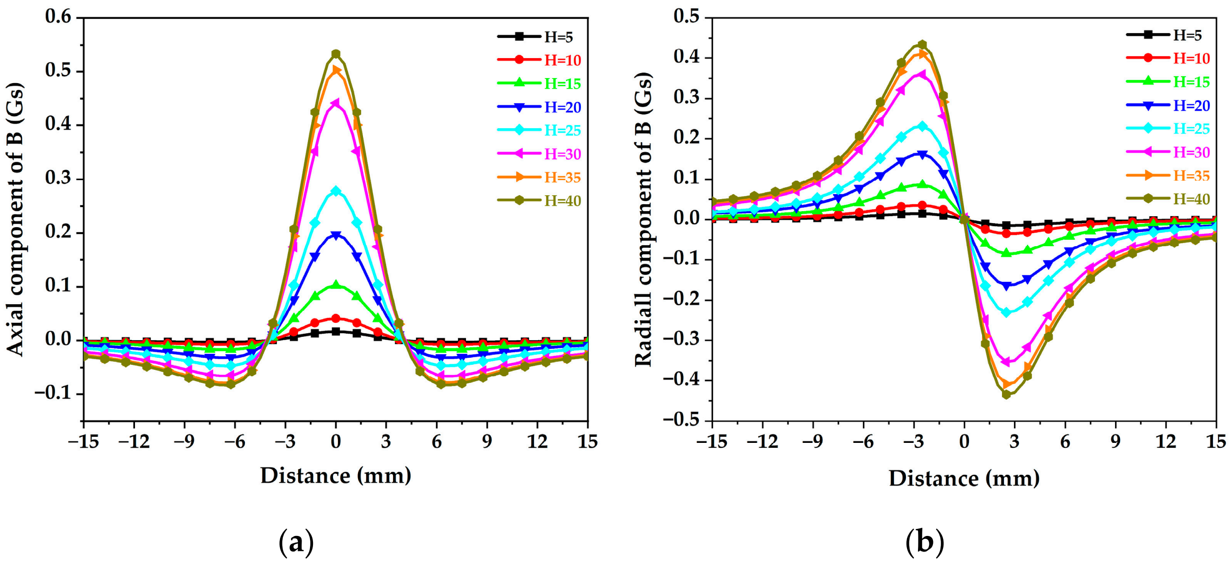

Figure 8. Changes in magnetic flux density with the changed axial height (H) of the magnet: (**a**) axial component of magnetic flux density; and (**b**) radial component of the magnetic flux density.

3.2.3. The Variable Is the Outer Diameter (OD) of the Magnet

As shown in Section 3.2.2, the simulation concludes that the larger the axial height (H) of the magnet, the greater its ability to detect defects. However, the value is too large, dramatically increasing the cost and increasing the overall size. Considering the design requirements, choose H = 30 mm, ID = 70 mm, and L = 30 mm; the magnet's outer diameter (OD) varies between 80 and 140 mm. The change curve of the defect characteristics as shown in Figure 9. The peak value of the defect MFL signal generally increases as L increases, and it decreases slightly when the outer diameter is 130 mm.

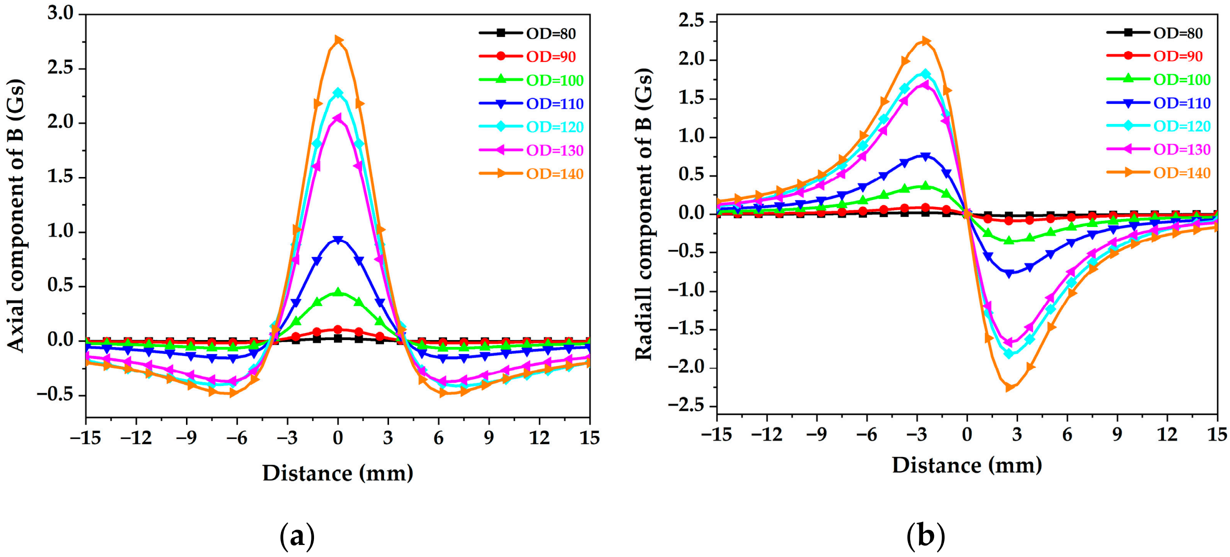

Figure 9. Changes in magnetic flux density with the changed outer diameter (OD) of the magnet: (**a**) axial component of magnetic flux density; and (**b**) radial component of the magnetic flux density.

3.2.4. The Variable Is the Inner Diameter (ID) of the Magnet

Select H = 30 mm, L = 30 mm, and OD = ID + 40 mm; the inner diameter (ID) of the magnet varies between 50 and 100 mm. The change curve of the defect characteristics is shown in Figure 10; when ID = 60 mm, the peak value of the defect MFL signal is the maximum, with the overall trend diminishing with the increase in ID.

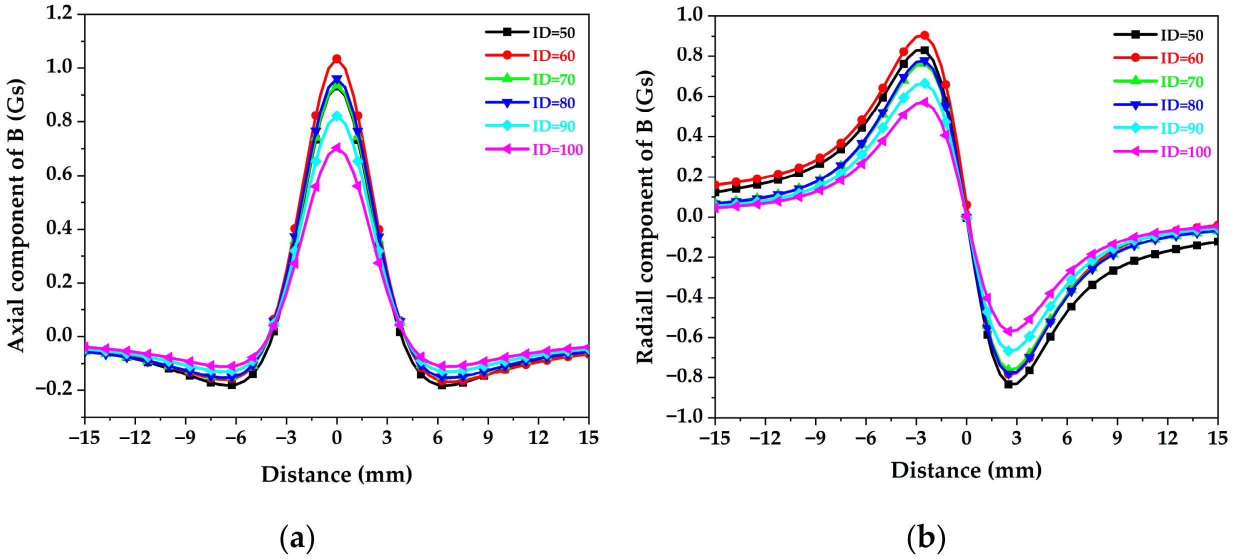

Figure 10. Changes in magnetic flux density with the changed inner diameter (ID) of the magnet: (**a**) axial component of magnetic flux density; and (**b**) radial component of the magnetic flux density.

3.3. Signal Characterization

For in-depth study and analysis of defect information, the features of the MFL signal are extracted, including the difference between the maximum and minimum values of the signal D (Dz and Dy), the span between the peak and the valley S (the span between the valley and the valley of the single peak Sz, the span between the peak and the peak of the double peak Sy), the envelope are $A = \frac{1}{2}\sum_{i=1}^{n}(B_{i-1}+B_i)d$, between the signal curve and the zero line (the absolute area Az and the absolute area Ay), where B_i is the flux density component of the ith data point, and d is the spacing between the two data points B_{i-1} and

B_i, shown in Figure 11, to analyze the variation patterns of the three eigenvalues under different variables.

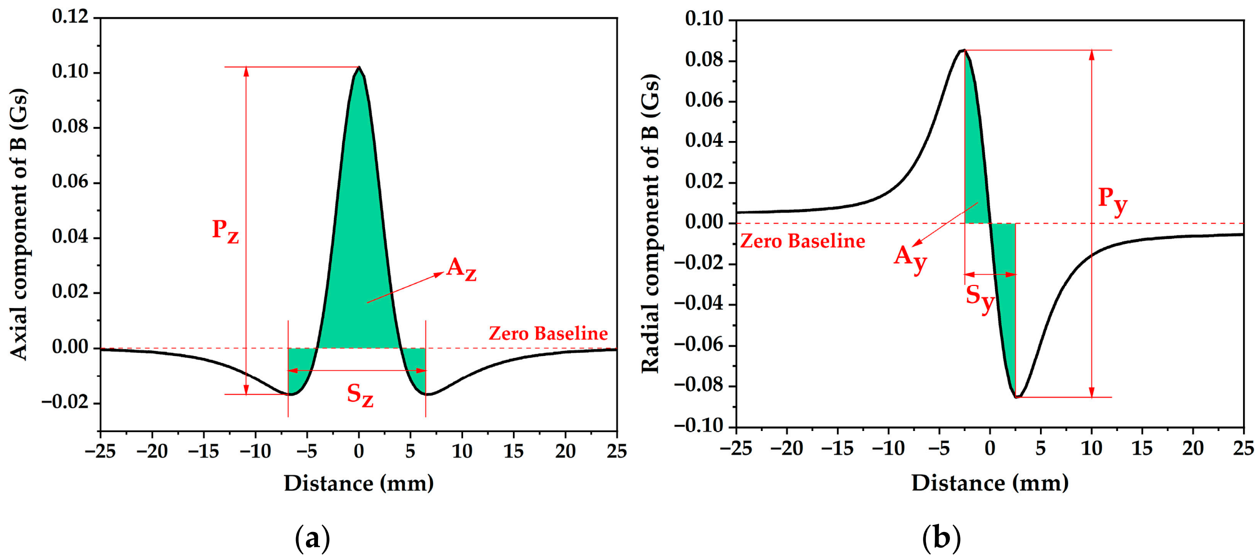

Figure 11. Defect signal characteristics: (**a**) Eigenvalues of the axial component of the signal; (**b**) Eigenvalues of the radial component of the signal.

Figure 12a–d shows, in order, the variation law of signal characteristics (D, S and A) when the variables are H, L, OD and ID. As shown in Figure 12a, Dz, Dy, Az, and Ay first increase and then decrease with increasing L, and the defect signal characteristics are maximal when L is 30 mm, whereas Sz and Sy are almost unchanged. Figure 12b shows that Dz, Dy, Az, and Ay gradually increase with an increase in H, while Sz and Sy remain essentially constant. In Figure 12c, Dz, Dy, Az, and Ay generally increase with increasing OD, while Sz and Sy are essentially constant. In Figure 12d, Dz, Dy, Az and Ay first increase and then gradually decrease with the increase in ID, while Sz and Sy are basically unchanged. This means that the change in the dimensions of the magnetizers (permanent magnets and cores) will not have an effect on S (Sy and Sz), but primarily on D (Dz and Dy) and A (Az and Ay) for the same defect. For better detection of the leakage field of defects, the length L of the magnetic core should not be too large, while the values of the thickness H and OD of the magnet should be larger, and the ID of the magnet should be smaller.

3.4. Preliminary Experimental Verification

In order to verify the simulation results, several magnetizer sizes were focused on, selecting for experimental comparison: (1) ID = 70 mm, OD = 100 mm, H = 15 mm, L = 10 mm; (2) ID = 70 mm, OD = 100 mm, H = 15 mm, L = 30 mm; (3) ID = 70 mm, OD = 100 mm, H = 15 mm, L = 60 mm; (4) ID = 70 mm, OD = 100 mm, H = 15 mm, L = 60 mm, and (5) ID = 70 mm, OD = 100 mm, H = 30 mm, L = 30 mm. As illustrated in Figure 13, a detection sensor was machined to size and an experimental system was developed to detect damage to the wire rope. A wire rope is magnetized to saturation by an open sensor. A leakage magnetic field is created on the surface of the magnetized wire rope when there is a defect. And the leakage magnetic field is captured by the inductor and passed through the data acquisition card, which converts it into electrical signal that can be analyzed by a PC analysis system. After the signal has been analyzed and processed by the data acquisition and test software, the curve of the detected signal is displayed on the screen in real-time.

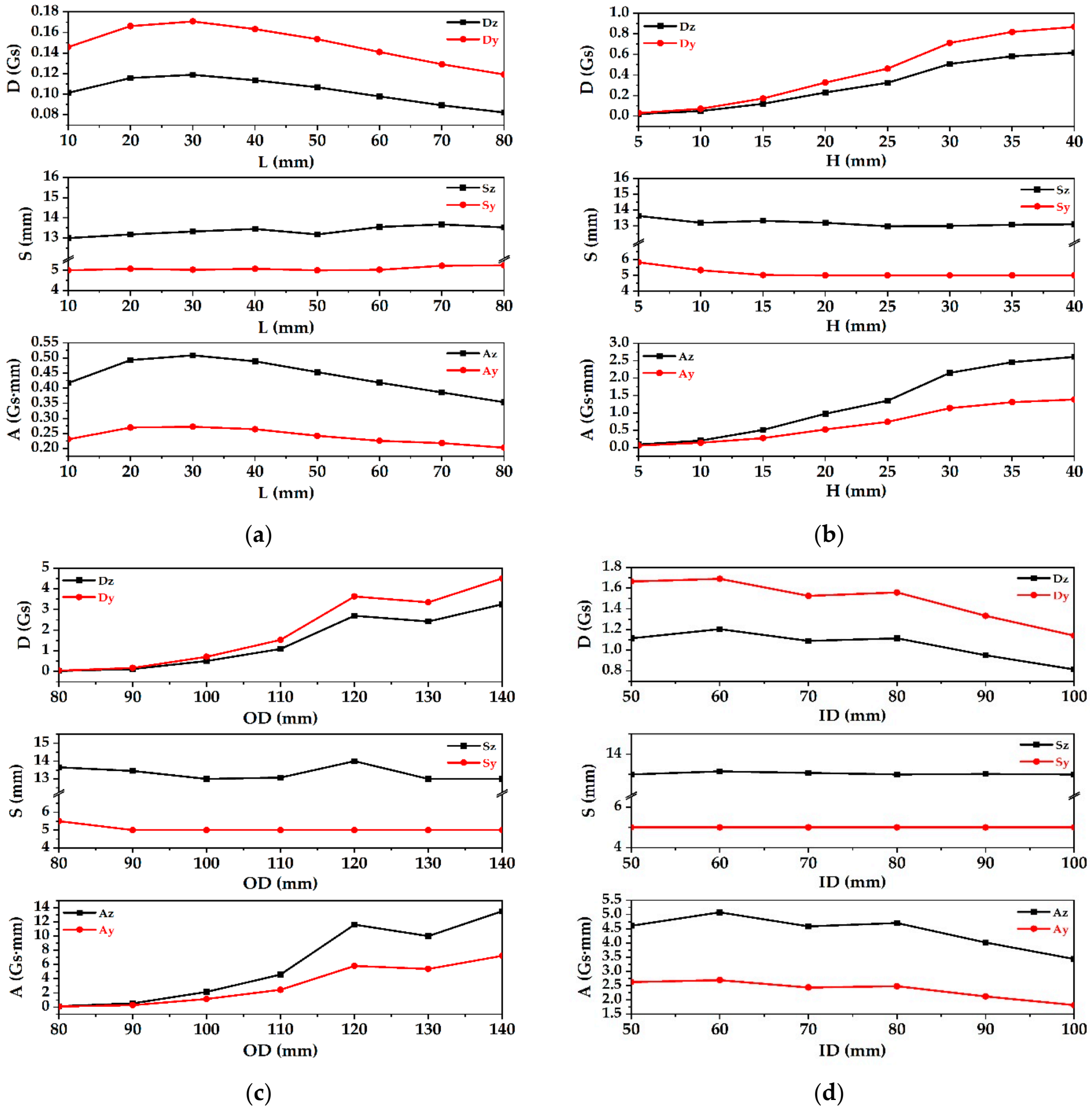

Figure 12. Defect signal characteristics under different variables: (**a**) defect signal characteristics under the variable L; (**b**) defect signal characteristics under the variable H; (**c**) defect signal characteristics under the variable OD; (**d**) defect signal characteristics under the variable ID.

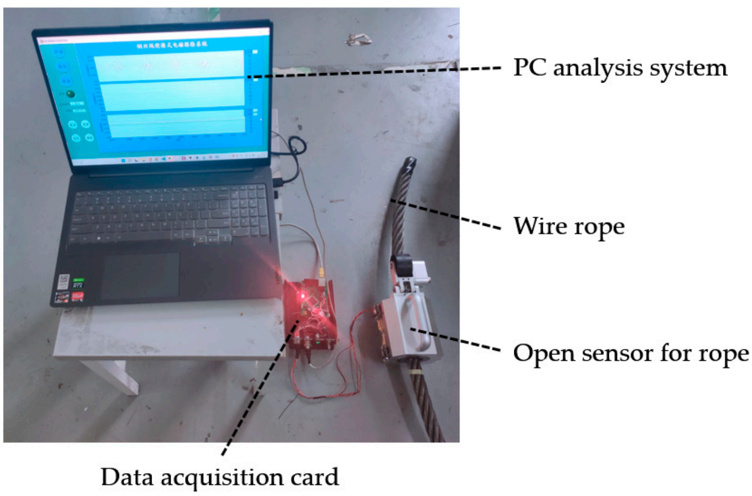

Figure 13. Experimental testing device.

Figure 14 shows two different types of damage on a wire rope with multiple broken wires and a single broken wire, highlighted with red circles. The detection device is fixed, and the wire rope is moved back and forth to spot sweep the damage of the wire rope. Figure 15 shows the experimental results of damage detection of wire rope under different magnetizer sizes. When ID = 70 mm and OD = 100 mm are unchanged, (1) the value of H = 15 mm remains unchanged, while L is 10 mm, 30 mm and 60 mm in order, then when L = 30 mm, the maximum amplitude of the damage signal is detected; (2) when L = 30 mm, while H is 15 mm and 30 mm, it is obvious that when H = 30 mm, the maximum amplitude of the damage signal is detected. Therefore, when designing the size of the magnetizer, the inner diameter of the magnet should be determined by the diameter of the wire rope, and the thickness and outer diameter of the magnet should be increased appropriately to reduce the length of the armature.

(**a**) (**b**)

Figure 14. Wire rope damage: (**a**) multiple broken wire damage; (**b**) single broken wire damage.

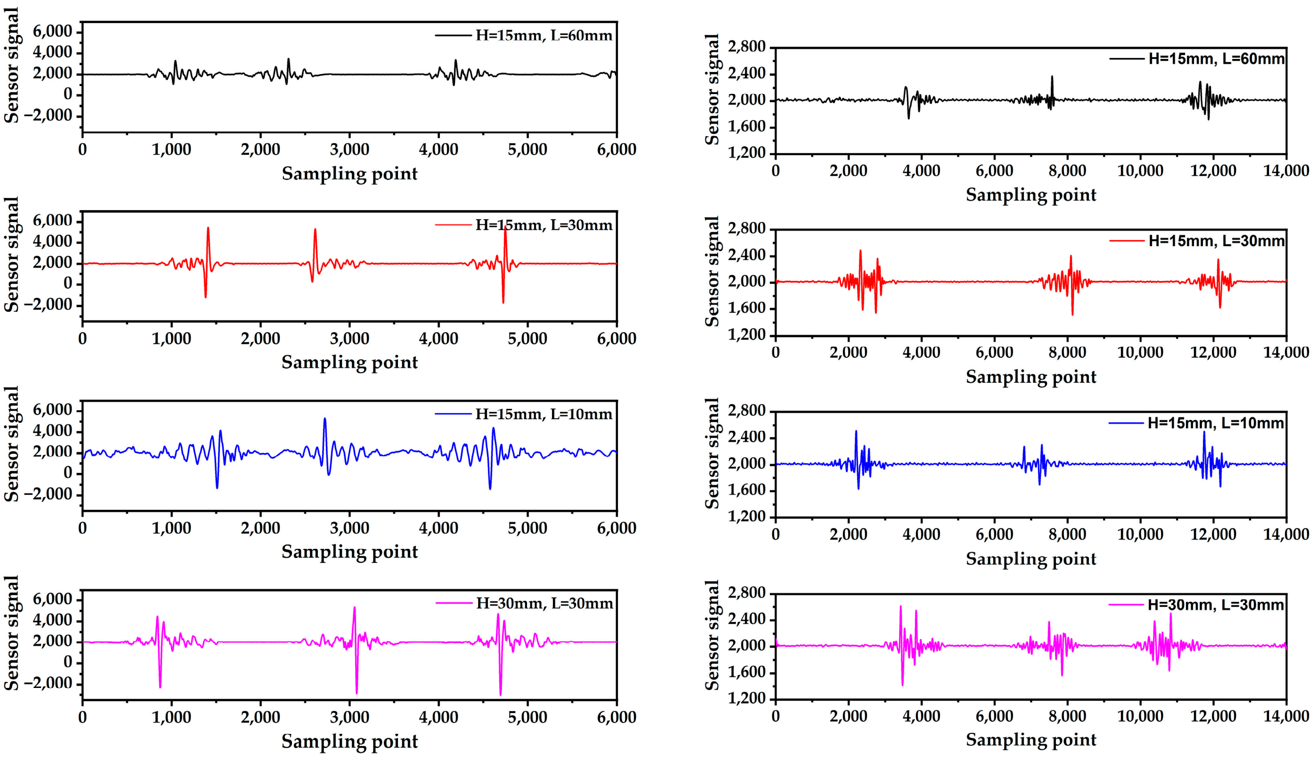

(**a**) (**b**)

Figure 15. Experimental results: (**a**) damage signal of multiple broken filaments; (**b**) damage signal of single broken filaments.

4. Key Techniques of the Method

On site, an on-line testing device is needed to send the open-loop permanent magnetization probe to the WMH wire rope so that the axis of the probe is aligned with the axis of the wire rope and it can float to track the movement of the wire rope in different directions. It is therefore designed to work in conjunction with the telescopic cylinder (electric cylinder) to bring the probe into the appropriate position; the working principle of this device is shown in Figure 16. The detection device is mainly composed of an inspection probe for opening and closing with clutch, a lifting cylinder (electric cylinder) and a rocker arm. At first, the lifting cylinder (electric cylinder) and the rocker arm will raise the probe to a specific position such that the probe axis coincides with the wire rope axis. The testing probe is controlled by a cylinder (electric cylinder) that slides the two parts of the probe along parallel linear guide rods to close or open them so that the probe is looped or disengaged from the wire rope.

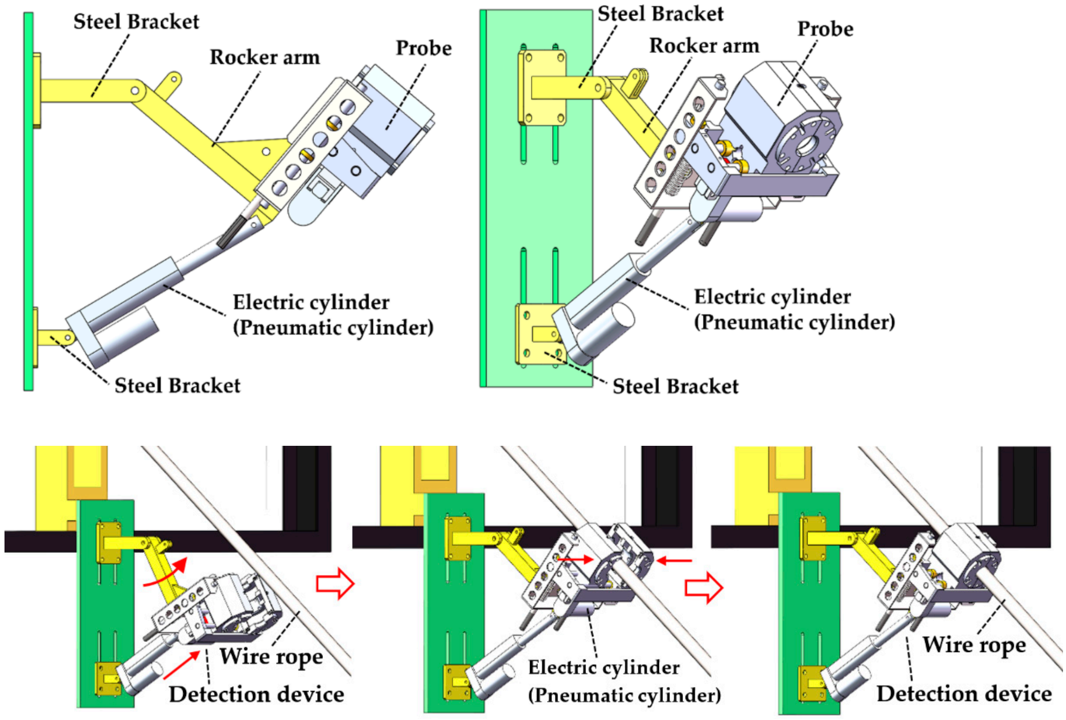

Figure 16. On-line testing devices.

The testing probe is closed to encircle the wire rope in the testing process and is driven by a floating tracking mechanism which allows the Y and Z degrees of freedom to be released so as to accommodate the vibration and wobble of the wire rope, thereby tracking the movements of the rope to detect. The floating tracking mechanism mainly consists of the first linear guide bar, bearing adapter plate, the second linear guide bar and the bottom plate, as shown in Figure 17. The testing probe controlled by the cylinder (electric cylinder) is installed on the first linear guide bar by the bearing, which is installed on the bearing adapter plate, and this part allows the testing probe to be freely moved in the Y direction. The bearing adapter plate is installed on the second linear guide bar by the bearing. The second linear guide bar is perpendicular to the first linear guide bar and is installed on a base plate connected to the rocker arm and the lifting cylinder (electric cylinder); this part can enable the probe to move freely in the Z direction. A spring is also connected between the bearing adapter plate and the bottom plate so that, on the one hand, the probe remains at the midpoint of the slide in the Z-direction of the tracking mechanism, and, on the other hand, the jitter amplitude in the Z-direction of the wire rope may be dynamically adjusted, cushioning and absorbing the changes in the attitude of the probe.

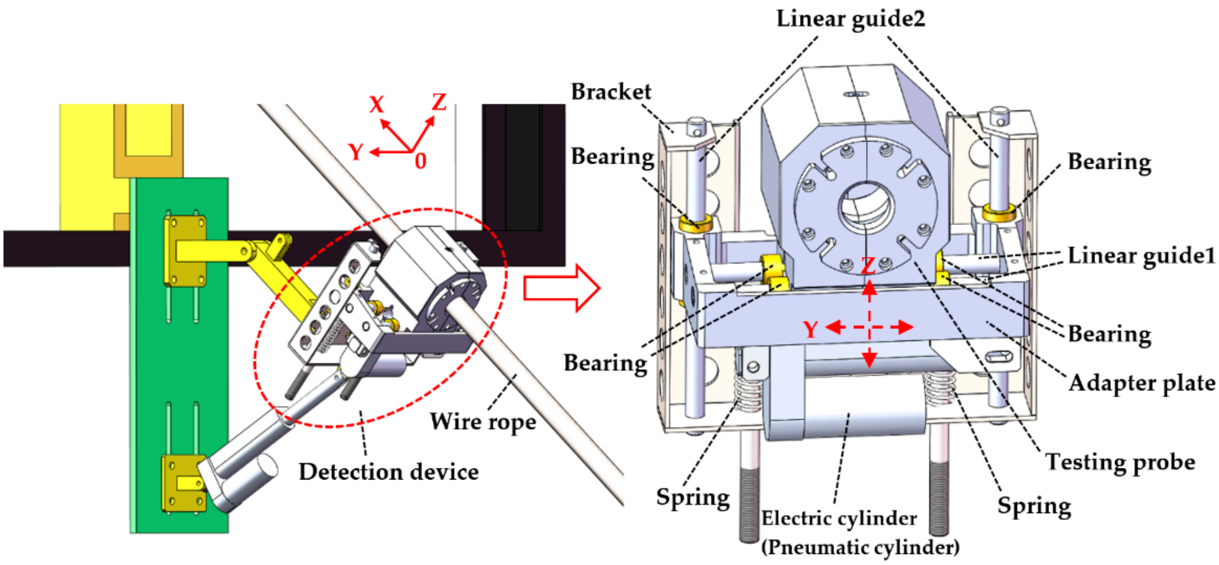

Figure 17. Test probes with floating tracking.

The probe is fitted with wear sleeves at both ends and the floating tracking mechanism accommodates rope wobble in any direction by leaving a small gap between the wear sleeves and the wire rope. The inner diameter of the magnetic sensitive probe shoe in the probe is usually 2–5 mm larger than the inner diameter of the wear-resistant sleeve, and the wear-resistant sleeve is used with the magnetic sensitive probe shoe to detect the corresponding specifications of the wire rope by replacing certain specifications of the probe shoe and the wear-resistant sleeve so as to realize the magnetic sensitive probe shoe to keep the fixed lifting away and non-contact detection with the wire rope.

The entity is machined and assembled according to the operating principle of the in-line testing device and the detection probe, as shown in Figure 18, and is mounted on a WMH wire rope running at high speed for real-time inspection.

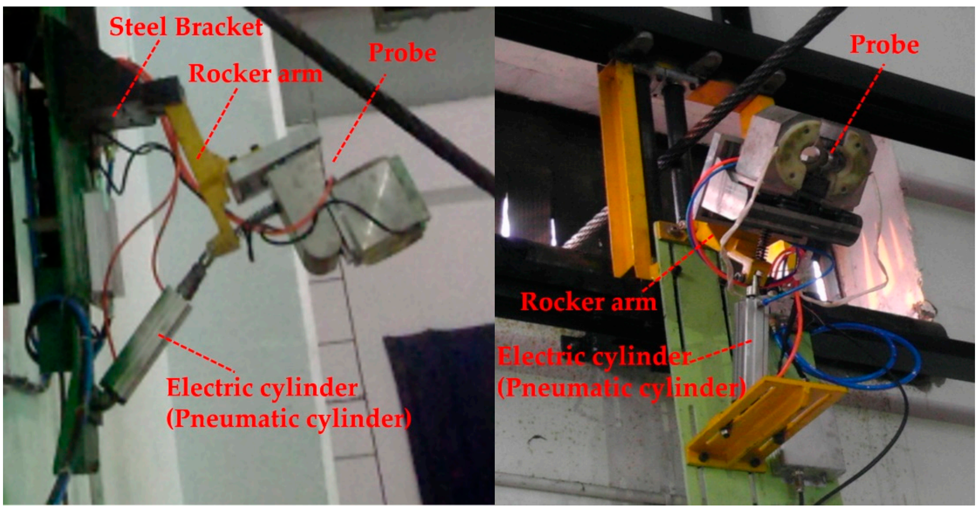

Figure 18. On-line testing device.

5. Testing Apparatus and Experiments

In order to evaluate the feasibility and practicality of the device, it was installed at the mine hoist site. Figure 19 indicates the installation principle of the device and on-site installation environment. A floating tracking on-line detection device utilizing an open-loop probe is attached to the guide wheel. The probe is driven by a cylinder (electric cylinder) to hold a co-axial line with the wire rope.

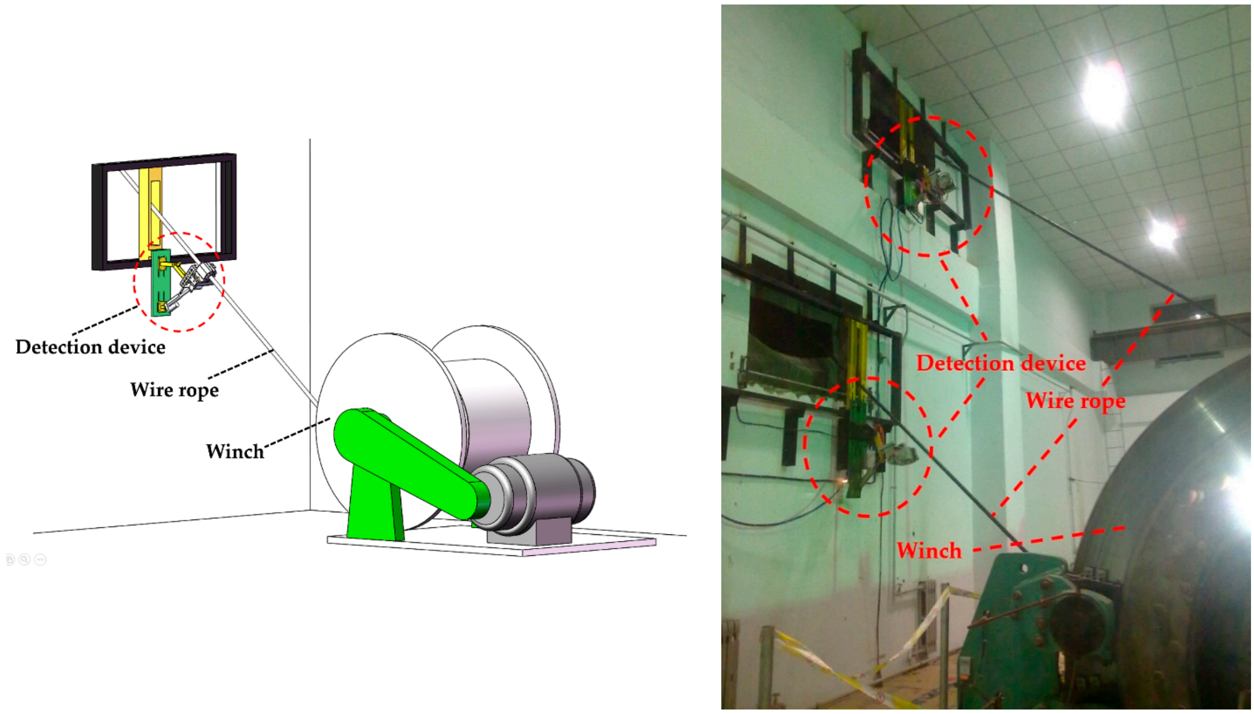

Figure 19. Installation of the device: (**a**) installation principle of the device; (**b**) on-site installation.

The test signals for a single broken wire and two adjacent broken wires in a wire rope are shown in Figure 20. The validity and feasibility of the newly proposed on-line test method and device for WMH wire ropes were confirmed by the characteristics of the test signals. They have a wide range of application prospects in the near future, particularly under complex operating conditions.

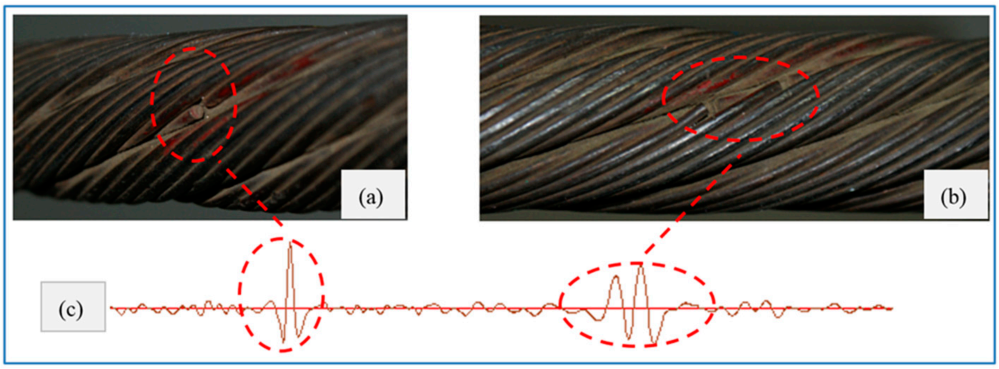

Figure 20. Specimen with defects: (**a**) single broken wire; (**b**) two adjacent broken wire; and (**c**) detection signals.

6. Conclusions

Based on MFL technology, a new probe for detecting WMH wire ropes was developed, and the performance of the testing probe was further enhanced by finite element analysis, which enables a large defect leakage field to be generated. Additionally, a new online MFL method was developed, as well as an on-line testing device coordinated with the new probe in order to ensure that the probe could detect defects in the wire rope without interference. A study of the results of the experiments revealed that the newly invented apparatus performed well for the on-line testing of wire rope, and this device can be expanded into multiple groups of the same device for detecting the requirements of multiple ropes. In addition, the apparatus may also be used for other similar occasions, including coiled tubing and coiled rod.

Furthermore, the quantitative relationship between the size of the detection magnetizer and the leakage field of the defect, including the diameter of the wire rope, the lifting distance and the type of defect, still requires further investigation. Research will be continued to determine the best match for the magnetizer size of the probe and the diameter of the particular wire rope. The relationship between the number of broken wires and the amplitude of the defect signals will also be studied.

Author Contributions: Conceptualization, Y.S. and X.J. (Xiaoyuan Jiang); methodology, X.J. (Xiaoyuan Jiang) and B.F.; software, X.J. (Xiaotian Jiang); validation, B.F. and M.L.; formal analysis, X.J. (Xiaoyuan Jiang) and M.L.; investigation, X.J. (Xiaoyuan Jiang); resources, Y.S.; data curation, X.J. (Xiaoyuan Jiang); writing—original draft preparation, X.J. (Xiaoyuan Jiang); writing—review and editing, B.F.; visualization, X.J. (Xiaoyuan Jiang); supervision, L.H. and Y.K.; project administration, R.L.; funding acquisition, R.L. All authors have read and agreed to the published version of the manuscript.

Funding: This research was funded from Research on Operation and Maintenance Technology of Balance Weight Wire Rope program, CHANGJIANG RIVER ADMINISTRATION of NAVIGATIONAL AFFAIRS, MOT, grant number SXHXGZ-2021-2.

Conflicts of Interest: The authors declare no conflict of interest.

References

1. Torkar, M.; Arzenšek, B. Failure of crane wire rope. *Eng. Fail. Anal.* **2002**, *9*, 227–233. [CrossRef]
2. Kotelnikov, V.; Sukhorukov, V. Rope NDT as means to raise safety of crane and elevator use. *Cinde J.* **2006**, *27*, 11.
3. Prawoto, Y.; Mazlan, R. Wire ropes: Computational, mechanical, and metallurgical properties under tension loading. *Comput. Mater. Sci.* **2012**, *56*, 174–178. [CrossRef]
4. Schrems, K.; Maclaren, D. Failure analysis of a mine hoist rope. *Eng. Fail. Anal.* **1997**, *4*, 25–38. [CrossRef]
5. Chaplin, C. Failure mechanisms in wire ropes. *Eng. Fail. Anal.* **1995**, *2*, 45–57. [CrossRef]
6. Cao, Y.; Zhang, D.; Wang, C.; Gu, Y.; Xu, D. A Novel Electromagnetic Method for Local Defects Inspection of Wire Rope. In Proceedings of the TENCON 2006—2006 IEEE Region 10 Conference, Hong Kong, China, 14–17 November 2006; pp. 14–17.
7. Jomdecha, C.; Prateepasen, A. Design of modified electromagnetic main-flux for steel wire rope inspection. *NDT E Int.* **2009**, *42*, 77–83. [CrossRef]
8. Katoh, M.; Masumoto, N.; Nishio, K.; Yamaguchi, T. Modeling of the yoke-magnetization in MFL-testing by finite elements. *NDT E Int.* **2003**, *36*, 479–486. [CrossRef]
9. Raišutis, R.; Kažys, R.; Mažeika, L.; Žukauskas, E.; Samaitis, V.; Jankauskas, A. Ultrasonic guided wave-based testing technique for inspection of multi-wire rope structures. *NDT E Int.* **2014**, *62*, 40–49. [CrossRef]
10. Wang, J.; Miao, C.; Wang, W.; Lu, X. Research of X-ray nondestructive detector for high-speed running conveyor belt with steel wire ropes. In *Electronic Imaging and Multimedia Technology V*; SPIE: Bellinghamb, WA, USA, 2007; pp. 482–490.
11. Bashir, I.; Walsh, J.; Thies, P.; Weller, S.; Blondel, P.; Johanning, L. Underwater acoustic emission monitoring—Experimental investigations and acoustic signature recognition of synthetic mooring ropes. *Appl. Acoust.* **2017**, *121*, 95–103. [CrossRef]
12. Bai, W.; Chai, M.; Li, L.; Li, Y.; Duan, Q. *Advances in Acoustic Emission Technology*; Springer: New York, NY, USA, 2014; pp. 217–224.
13. Cao, Q.; Liu, D.; He, Y.; Zhou, J.; Codrington, J. Nondestructive and quantitative evaluation of wire rope based on radial basis function neural network using eddy current inspection. *NDT E Int.* **2012**, *46*, 7–13. [CrossRef]
14. Liu, S.; Sun, Y.; Jiang, X.; Kang, Y. A Review of Wire Rope Detection Methods, Sensors and Signal Processing Techniques. *J. Nondestruct. Eval.* **2020**, *39*, 85. [CrossRef]
15. Zhou, P.; Zhou, G.; Zhu, Z.; He, Z.; Ding, X.; Tang, C. A Review of Non-Destructive Damage Detection Methods for Steel Wire Ropes. *Appl. Sci.* **2019**, *9*, 2771. [CrossRef]
16. Wu, B.; Wang, Y.; Liu, X.; He, C. A novel TMR-based MFL sensor for steel wire rope inspection using the orthogonal test method. *Smart Mater. Struct.* **2015**, *24*, 075007. [CrossRef]
17. Jiang, X.; Xia, Y. A GA based optimized designation of detection sensor for broken steel stranded wire faults in ACSR. In *2010 International Conference on High Voltage Engineering and Application*; IEEE: New Orleans, LA, USA, 2022; pp. 672–675.
18. Yan, X.; Zhang, D.; Zhao, F. Improve the signal to noise ratio and installation convenience of the inductive coil for wire rope nondestructive testing. *NDT E Int.* **2017**, *92*, 221–227. [CrossRef]
19. Zhang, Y.; Jing, L.; Xu, W.; Zhan, W.; Tan, J. A Sensor for Broken Wire Detection of Steel Wire Ropes Based on the Magnetic Concentrating Principle. *Sensors* **2019**, *19*, 3763. [CrossRef]
20. Pan, S.; Zhang, D.; Zhang, E. Nondestructive Testing for Shallow Defect of Ferromagnetic Objects Based on Magnetic Probe Structure. *IEEE Trans. Magn.* **2018**, *54*, 4002406. [CrossRef]

21. Zhang, D.; Zhang, E.; Pan, S. A new signal processing method for the nondestructive testing of a steel wire rope using a small device. *NDT E Int.* **2020**, *114*, 102299. [CrossRef]
22. Wang, H.; Tian, J.; Li, X.; Lv, X. Inspection of Mine Wire Rope Using Magnetic Aggregation Bridge Based on Magnetic Resistance Sensor Array. *IEEE Trans. Instrum. Meas.* **2020**, *69*, 7437–7448. [CrossRef]
23. Singh, W.; Rao, B.; Thirunavukkarasu, S.; Jayakumar, T. Flexible GMR Sensor Array for Magnetic Flux Leakage Testing of Steel Track Ropes. *J. Sens.* **2012**, *2012*, 129074. [CrossRef]
24. Gu, W.; Chu, J. A transducer made up of fluxgate sensors for testing wire rope defects. *IEEE Trans. Instrum. Meas.* **2002**, *51*, 120–124. [CrossRef]
25. Sun, Y.; Liu, S.; Li, R.; Ye, Z.; Kang, Y.; Chen, S. A new magnetic flux leakage sensor based on open magnetizing method and its on-line automated structural health monitoring methodology. *Struct. Health Monit.* **2015**, *14*, 583–603. [CrossRef]
26. Xu, J.; Wu, X.; Cheng, C.; Ben, A. A Magnetic Flux Leakage and Magnetostrictive Guided Wave Hybrid Transducer for Detecting Bridge Cables. *Sensors* **2012**, *12*, 518–533. [CrossRef] [PubMed]
27. Zhang, D.; Zhang, E.; Yan, X. Quantitative method for detecting internal and surface defects in wire rope. *NDT E Int.* **2021**, *119*, 102405. [CrossRef]
28. Sun, Y.; Liu, S.; He, L.; Kang, Y. A new detection sensor for wire rope based on open magnetization method. *Mater. Eval.* **2017**, *75*, 501–509.
29. Hua, G.; Wang, H.; Chen, F.; Lu, Y.; Xu, Z.; Tian, J.; Zhou, B. Improving SNR of MFL Signal in Flaw Detection of Coal Mine Wire Ropes. In Proceedings of the 2009 2nd International Congress on Image and Signal Processing, Tianjin, China, 17–19 October 2009; pp. 1–6.
30. Azad, A.; Kim, N. Design and Optimization of an MFL Coil Sensor Apparatus Based on Numerical Survey. *Sensors* **2019**, *19*, 4869. [CrossRef]